Braz J Phys (2014) 44:645–652
DOI 10.1007/s13538-014-0244-4

CONDENSED MATTER

Effects of Bi_2O_3 Addition in Micro- and Nanoscale on the Structural and Electrical Properties of $Zn_{1-x}Bi_xO$ varistors

A. Sedky

Received: 21 May 2014 / Published online: 20 August 2014

Abstract Two similar sets of $Zn_{1-x}Bi_xO$ ceramic varistors with various x values ($0.00 \leq x \leq 0.20$) have been prepared by using Bi_2O_3 additions with two different sizes. In the first set, Bi_2O_3 nanoparticles (≈200 nm) were used, while Bi_2O_3 microparticles (≈5 μm) were used in the second set. It was found that addition of Bi up to 5 % for both sets did not affect the wurtzite-type hexagonal structure of ZnO, but with increasing Bi above 5 %, some unknown lines were clearly observed in XRD spectra. The grain sizes are increased in both sets with increasing Bi content up to 2.5 %, followed by a decrease with further increase of Bi up to 20 %, and their values for microparticle additions were larger than that of the sets containing nanoparticle additions. Two nonlinear regions were formed in the I–V curves of ZnO due to Bi_2O_3 nanoparticle additions above 5 %. However, this behavior was completely absent in the samples containing Bi_2O_3 microparticles. Moreover, the breakdown field and nonlinear coefficient decreased with Bi_2O_3 addition up to 5 % for both sets, followed by an increase with further increase of Bi up to 20 %, and their values were higher for nanoparticle additions than that of microparticles. A reverse behavior was recorded for the electrical conductivity. The results have been discussed in terms of Bi_2O_3 nanosize grains which may be localized at the grain boundaries of ZnO ceramics.

Keywords Ceramics · Chemical synthesis · X-ray diffraction · Electrical properties · Transport properties

A. Sedky (✉)
Physics Department, Faculty of Science, Assiut University, Assiut 71515, Egypt
e-mail: sedky1960@yahoo.com

A. Sedky
Physics Department, Faculty of Science, King Faisal University, Al-Hassa 31982P.O.B 400, Saudi Arabia

1 Introduction

Zinc oxide (ZnO) has a wurtzite-type hexagonal structure with lattice parameters (a=3.249 Å and c=5.206 Å). ZnO is an n-type semiconductor and has a wide band gap of 3.2 eV [1, 2]. ZnO has a wide range of applications in gas sensors, piezoelectric transducers, solar cells, and varistors [1–4]. This is because ZnO ceramics is a multiphase structure which exhibits highly nonlinear current–voltage characteristics due to electrostatic potential barrier formed at grain boundaries [5–8]. Regarding ZnO varistor, it has high-energy absorption capability against various surges, and it is extensively used as a protective device. It has a super fast response to overvoltage transients and clamp transients at nanosecond speed without being destroyed [2].

Since the invention of ZnO varistors in 1970 [9], a considerable number of investigations have been carried out into the nonlinear behavior obtained in its I–V characteristics. The ZnO varistors are typically fabricated by sintering of ZnO with other metal oxides as additives. These additives are the main tools which have been used to test change the nonlinear response and the stability of ZnO varistors [10–16]. Several efforts have been carried out to describe the influence of Bi_2O_3 addition on the microstructure and electrical properties of ZnO. The authors pointed out that a very low amount of Bi_2O_3 is lost during sintering at high temperature, but they did not give its quantity [17–19]. Few reports have been concerned with the assessment of Bi_2O_3 vaporization during the sintering process. A loss of 19 wt% of Bi_2O_3 has been recorded for the process conducted at 1,150 °C for 90 min by emission spectroscopy [20–22]. The other reports found that all interlayers in Bi-doped polycrystalline ZnO take on a thin, amorphous and rich nanostructure phase structure after being annealed above eutectic temperature [23].

Nanotechnology is an enabling technology, with high potential impact on virtually all fields of mankind activity. The rapid progress of nanoscience creates demands for the detailed characterization of matter on the nanometer scale, which provide new capabilities for the analysis of a large variety of properties related to lower dimensionality and local structure, reaching down to single atoms and molecules. Nanoparticles are currently the focus of intense investigations due to their potential for revolutionary technological applications. The phenomena and properties behind these applications are unique to nanodimensions such as quantum confinement effects and enhanced surface to volume ratio.

Normally, the nanostructured materials often show novel physical properties compared to those of bulk due to their peculiar characteristics and size effects. In the recent works, nanoparticles of metal oxides have been a subject of a number of research efforts due to their expected unusual properties connected with the nanostructure regime [24, 25]. Moreover, two nonlinear regions in the I–V curves of ZnO with Fe_2O_3 nanoparticles additions above 10 % were reported in [26]. The breakdown field was increased up to 7,900 V/cm, and the electrical conductivity was improved by Fe_2O_3 additions up to 10 %. However, further increase of Fe_2O_3 up to 50 % resulted in a decrease in electrical conductivity.

In this paper, we report on the structure and morphology evolution of two similar sets of $Zn_{1-x}Bi_xO$ ceramic samples with various x values. The samples were examined using X-ray diffraction, high-field scanning electron microscope, and dc electrical measurements.

2 Experimental Details

Two similar sets of $Zn_{1-x}Bi_xO$ ceramic samples with various x values (x=0.00, 2.5, 5, 10, and 20 %) were prepared using a solid-state reaction method with Bi_2O_3 additions of two different sizes. In the first set, Bi_2O_3 nanoparticles (≈200 nm) were used, while Bi_2O_3 microparticles (≈5 μm) were used in the second set. The powders of ZnO and Bi_2O_3 (Aldrich, 99.999 % purity) were thoroughly ground, mixed in required proportions, and calcined at 900 °C in air for a period of 12 h and then quenched in air down to room temperature. The resulting powders were reground and pressed into pellets of 1-cm diameter and 0.3-cm thickness. Finally, these pellets were sintered at a temperature of 1,000 °C for 10 h in air and then quenched in air down to room temperature. The bulk density of the samples was measured in terms of their weight and volume. The phase purity of the samples was examined by using X-ray diffractometer (XRD, Siemens D-500) with the Cu Kα radiation of 1.541838 Å. The surface morphology of the samples was examined using field emission scanning electron microscope (FESEM). The I–V characteristics of the samples were obtained with an electrometer (model 6517, Keithley, 5 kV, 300 mA) dc power supply and digital multimeter. The samples were thoroughly polished and sandwiched between two copper electrodes, and the current was measured as a function of the applied voltage at room temperature. High quality silver paint was used on the sample surfaces for electrical contacts.

3 Results and Discussion

The bulk density of the samples, listed in Tables 1 and 2, has increased with Bi additions up to 0.20 %, and the values for "nanoparticle samples" are higher than that of "microparticles." They range from 76.3 to 97.92 % of the theoretical density for ZnO (5.78 g/cm^3) [27]. The XRD patterns of the samples shown in Fig. 1a, b indicate that the addition of Bi up to 5 % does not influence the well-known peaks related to hexagonal wurtzite structure of ZnO ceramics. With Bi content increasing above 5 %, some unknown lines related to BiO are observed, which may result from the replacement of Zn by Bi. This is because some amount of Bi is localized at the interlattice spacings and generates these extra lines. To further clarify that Bi is substituted for Zn in a unit cell, the lattice parameters a and c have been calculated and listed in Tables 1 and 2. It has been found that these parameters increase with Bi addition up to 5 % followed by a decrease with further increase of Bi up to 20 %. The values of lattice parameters are between 3.136 and 3.235 Å for a parameter and between 5.093 and 5.200 Å for the c parameter in agreement with the reported data [15, 27]. However, in a real ZnO crystal, the wurtzite structure deviates from the ideal arrangement by changing the c/a ratio for hexagonal distortion or the U parameter. U parameter is defined as a length of a bond parallel to the c-axis, in units of c, and c/a is the deviation from that of the ideal wurtzite crystal structure. U=0.333 $(a/c)^2$+0.25 [28], and it is equal to 0.375 in an ideal wurtzite structure in fractional coordinates.

The a/c ratio and u parameter versus Bi content are shown in Table 1. The a/c values are varying from 0.623 to 0.629 for nanoparticle samples and from 0.623 to 0.610 for microparticle samples. The u values are between 0.374 and 0.379 for microparticles and from 0.379 to 0.382 for "nanoparticles." It should be pointed out that a strong correlation exists between the c/a ratio and the u parameter, i.e., when c/a ratio increases, u parameter decreases in such a way that the four tetrahedral distances remain nearly constant in spite of distortion of tetrahedral angles, which may be due to long-range polar interactions. The deviation from that of the ideal wurtzite crystal is probably due to lattice stability and iconicity. The point defects such as zinc sites, oxygen vacancies, and threading dislocations also cause an increase of the lattice

Table 1 Density, grain size, breakdown field, lattice parameter, u parameter, and nonlinear coefficients for Bi_2O_3 microadditions

Bi content (%)	ρ (gm/cm^3)	D (μm)	D_{101} (nm)	a (Å)	c (Å)	u	E_B (V/cm)	α_2	α_4
0.00	4.41	2.21	86.51	3.208	5.145	0.379	1,580	18.7	–
2.5	4.59	2.46	74.22	3.218	5.174	0.378	178	4.7	–
5	4.95	2.24	86.41	3.222	5.200	0.377	330	6.8	–
10	5.11	2.01	89.98	3.187	5.171	0.376	980	8.2	–
20	5.28	1.75	90.84	3.136	5.137	0.376	2,866	10.2	–

constant, albeit to a lesser extent in the hetero-epitaxial layers [29].

The FESEM images shown in Fig. 2a indicate that the grains and their boundaries are uniformly distributed over the matrix structure. The average grain size versus Bi content shown in Fig. 2b increases with Bi addition up to 2.5 %, followed by a decrease with further increase of Bi content up to 20 %. Their values of grain size, listed in Tables 1 and 2, are lower in nanoparticle samples than that of microparticles. They have decreased as a result of Bi additions to 1.75 μm for microparticle samples and to 1.43 μm for nanoparticle.

On the other hand, the distribution of nanoparticle size D_{101} is evaluated in terms of X-ray line broadening described by Scherer's equation $D_{hkl} = \frac{k\lambda}{\Delta\theta\cos\theta}$ [27], where λ is the X-ray wavelength (λ=1.5418 Å), Δθ is the half maximum line width, θ is the Bragg angle, and K is the constant (K=0.9 for this type of ceramics). D_{101} versus Bi contents are listed in Tables 1 and 2, and their values are decreased with Bi addition up to 2.5 %, followed by an increase with further increase of Bi content up to 20 %. Although D_{101} values are lower in nanoparticle samples than that of microparticles, the behavior is different with that of SEM microsize data.

Figure 3a, b illustrates the room temperature I–V characteristics for the two sets of $Zn_{1-x}Bi_xO$ samples. Three different regions can be observed in the I–V curves for Bi=0.00; 2.5 and 5 % for both sets. The first and third regions show typical ohmic behavior, while the second region is nonlinear. With increasing Bi content above 5 % (10 and 20 %), five different regions can be observed in the I–V curves of the nanoparticle samples. This behavior does not exist in the I–V curves of microparticle samples. Moreover, two different nonlinear regions can be observed in the I–V curves of the samples with higher Bi content: the first in the low field region and the other in the high-field region. This mechanism is very useful for the operation of ZnO varistors both in the low and high-field regions at the same time (i.e., two reversible lines). The breakdown field E_B is usually considered as a field for which the current flowing through a varistor is 1 mA/cm^2 [30, 31]. Figure 4a shows E_B against Bi content for both sets, and the corresponding values are listed in Tables 1 and 2. E_B decreases for 2.5 % of Bi addition, followed by an increase with further increase of Bi up to 20 %, and its values are higher in nanoparticle samples than that of microparticles. The addition of Bi_2O_3 nanoparticles to ZnO improves the E_B of ZnO varistor by 2.88 times in comparison to E_B of a varistor made of pure ZnO. E_B is improved from 1,580 V/cm for ZnO to 2,866 V/cm for microparticle samples and up to 4,536 for nanoparticle samples. This means that the addition of Bi to a ZnO varistor shifts the breakdown fields to higher values. This may be attributed to the creation of point defects due to solid solution of Bi_2O_3 in the host lattice of ZnO varistors. The effective activation energy for the conduction as well as the potential barrier height is raised. This is because the addition of Bi_2O_3 contributes to the barrier formation at the grain–grain interface [32]. A similar behavior has been reported for ZnO varistors doped by Fe_2O_3 nanoparticles [26]. Therefore, the improvement in the values of E_B by Bi addition is expected in our present samples.

The current–voltage relation of a varistor is given by [30, 31]:

$$J = (E/C)^{\alpha}, \tag{1}$$

where J is the current density, E is the applied electric field, C is a proportionality constant corresponding to the resistance of

Table 2 Density, grain size, breakdown field, lattice parameters, u parameter, and nonlinear coefficients for Bi_2O_3 nanoadditions

Bi content (%)	ρ (gm/cm^3)	D (μm)	D_{101} (nm)	a (Å)	c (Å)	u	E_B (V/cm)	α_2	α_4
0.00	4.41	2.21	86.51	3.208	5.145	0.379	1,580	18.7	–
2.5	4.67	2.32	61.64	3.226	5.160	0.380	1,300	12.3	–
5	5.07	1.83	79.17	3.235	5.165	0.380	1,818	15.2	–
10	5.32	1.64	86.08	3.217	5.118	0.381	3,660	20.1	12.35
20	5.66	1.43	87.72	3.205	5.093	0.382	4,536	23.4	13.85

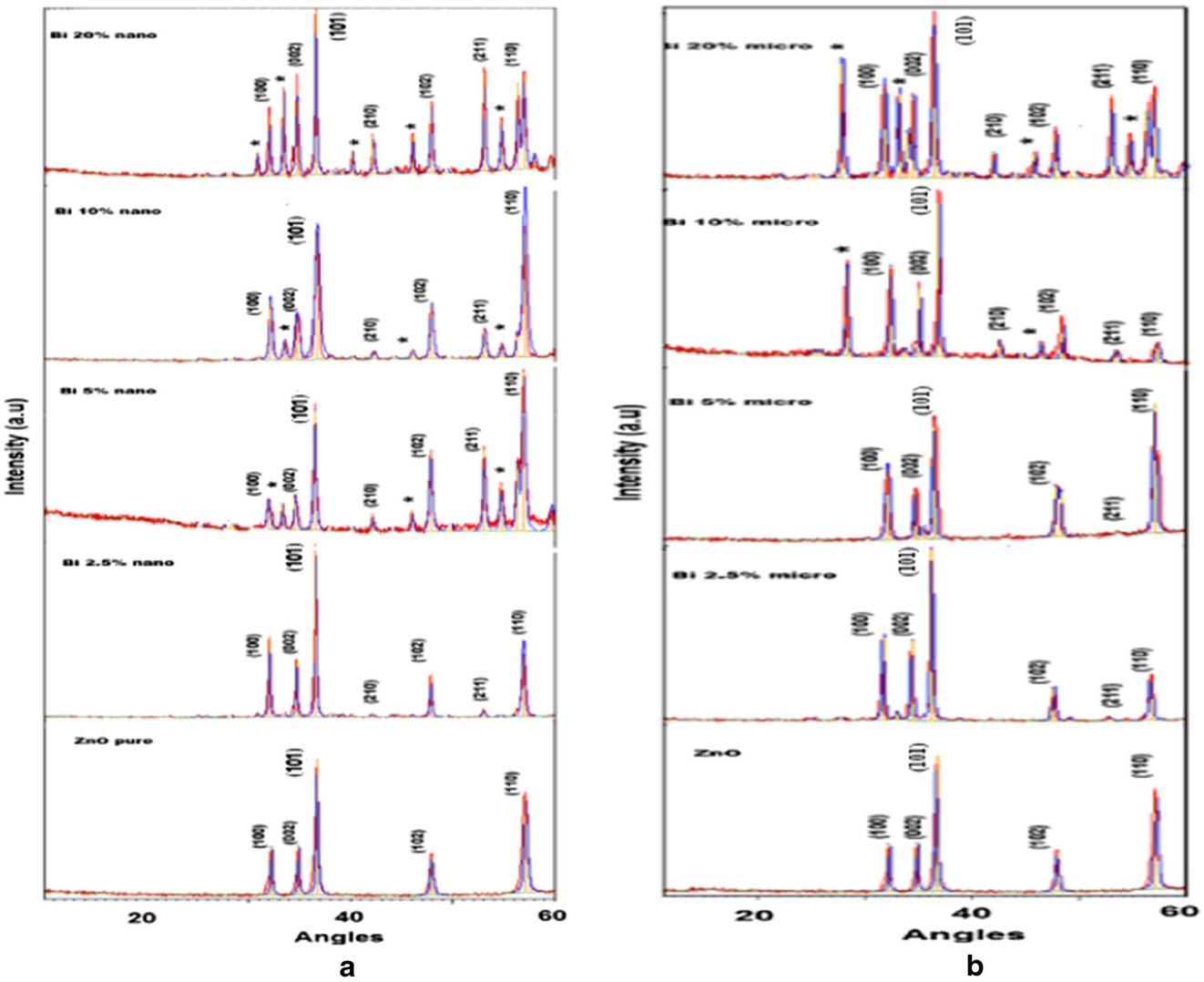

Fig. 1 **a** XRD patterns for Zn_{1-x} Bi_xO (Bi_2O_3 microparticles) samples. **b** XRD patterns for Zn_{1-x} Bi_xO (Bi_2O_3 nanoparticles) samples

ohmic resistor (nonlinear resistance), and α is the nonlinear coefficient. The current–voltage curves are plotted on a log–log scale from which the slope of the curve gives the value of α [9]. The variation of α versus Bi content across the second region is shown in Fig. 4b. Corresponding values are listed in Tables 1 and 2. It is clear that the values of α decrease for 2.5 % Bi additions, followed by an increase with further increase of Bi up to 20 %, but their values for nanoparticle samples are higher than that of microparticles [14]. Moreover, the values of α improved from 18.7 to 23.4 by 50 % Bi nanoparticle additions.

It is well known that electrical conductivity of ZnO samples is controlled by the intrinsic defects generated at high temperature and by the presence of dopants added to ZnO. During a cooling process, these defects tend to migrate to the grain boundaries and annihilate (intrinsic defects) or are exsolved if their solubility limit is attained (extrinsic effects). This migration process is normally slow and thermally activated, and at a temperature below a sintering temperature, only the defects near the grain boundaries are effectively eliminated [33]. The resulting concentration profiles/distributions considerably affect the electrical properties of ZnO varistors [34]. In order to avoid this process, the examined samples were quenched from sintering temperature down to room temperature. At room temperature, the defects are homogeneously distributed in the material, and their concentration is the same as those at the sintering temperature. However, the electrical conductivity σ at room temperature has been calculated across the first ohmic region by using the well-known relation, $J=\sigma$ E and is shown in Fig. 5. It is evident that σ increases as a result of Bi additions up to 2.5 %, followed by a decrease with further increase of Bi up to 20 %, and its values are higher in microparticle samples than that of nanoparticles. This is similar to the relation of grain size versus Bi content shown in Fig. 2b (directly proportional) but different from the dependence of breakdown

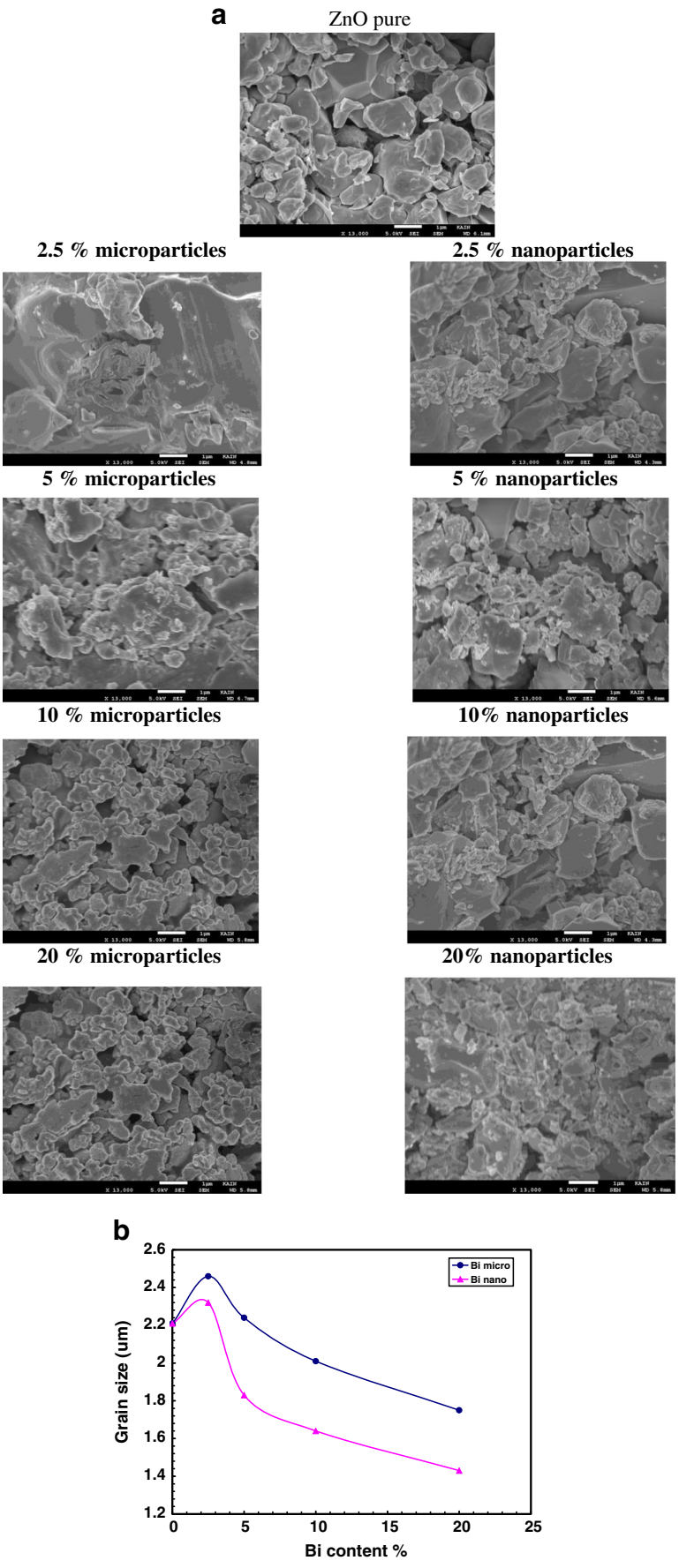

Fig. 2 **a** FESEM images for $Zn_{1-x}Bi_xO$ samples. **b** Average grain size versus Bi_2O_3 for $Zn_{1-x}Bi_xO$ samples

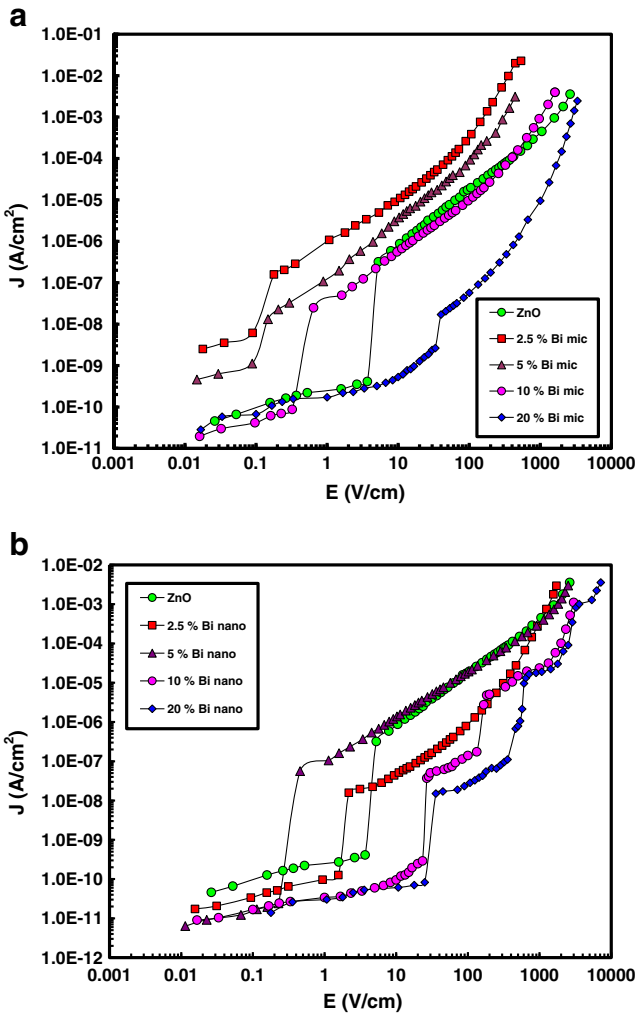

Fig. 3 **a** I–V characteristics for Zn_{1-x} Bi_xO (Bi_2O_3 microparticles) samples. **b** I–V characteristics for Zn_{1-x} Bi_xO (Bi_2O_3 nanoparticles) samples

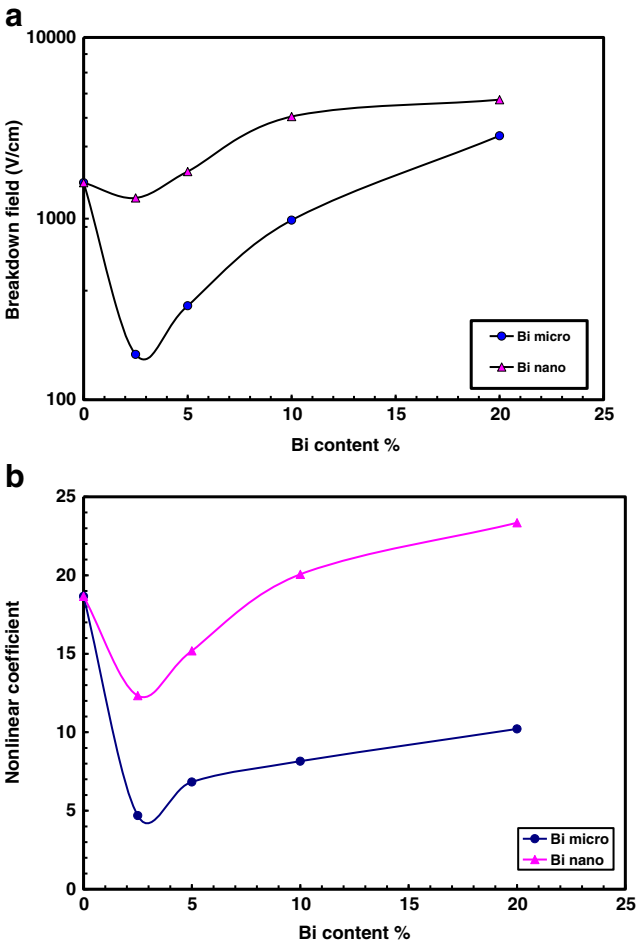

Fig. 4 **a** Breakdown field versus Bi content for Zn_{1-x} Bi_xO samples. **b** Nonlinear coefficient versus Bi content for Zn_{1-x} Bi_xO samples

field and nonlinear coefficient on Bi content (inversely proportional) [35]. This means that the breakdown field and nonlinear coefficient could be improved by decreasing the size of ZnO grains, but in such case, the electrical conductivity is decreased, which is not desirable in most of ZnO applications. The dependence of the above parameters on the grain size suggests a beneficial role of Bi nanoadditions into the ZnO, and further work is required to elucidate the present results.

To understand the mechanism of Bi reaction with Zn in the ZnO structure, let us now discuss the expected reactions as follows.

Neutral interstitial Zn atom undergoes ionization first as [15]:

$$Zn^0 \rightarrow Zn^+ + e^-, \text{ and secondly is ionized as :}$$
$$Zn^+ \rightarrow Zn^{2+} + e^-.$$

Such free electrons move to the conduction band of ZnO and enhance the conductivity of ZnO. The conductivity of ZnO can be also increased by extrinsic defects such as Bi^{3+} at Zn sites. In Zn^{2+} substituted by Bi^{3+}, some of the free electrons are released and raise the conductivity of ZnO through increasing the electron density/concentration. Therefore, the

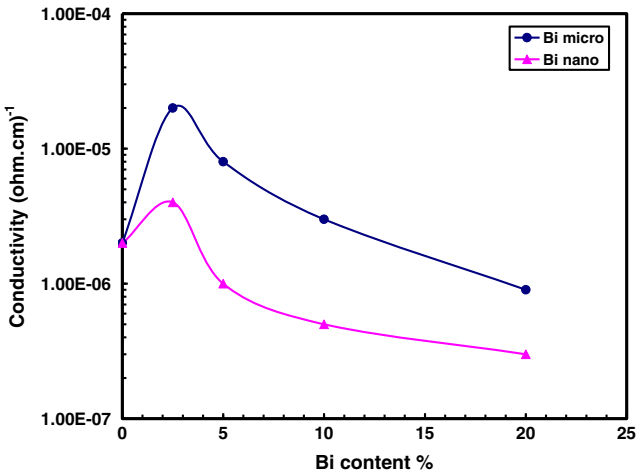

Fig. 5 Electrical conductivity at room temperature versus Bi content for Zn_{1-x} Bi_xO samples

interaction mechanism between Bi and Zn can be as follows [31, 34]:

$$\tfrac{1}{2}\,Bi_2O_3 \rightarrow \tfrac{1}{4}\,O_2 + Bi^Z + e + ZnO. \quad (2)$$

Bi^Z is the ionized Bi atom in Zn atom substitution site since Bi acts as a donor, so Bi^{3+} moves to Zn sites, and some additional free electrons are released. This reaction is consistent with the behavior of conductivity in the under-doped region (Bi≤2.5 %), but with increasing Bi addition above 2.5 %, Bi^{3+} can enter the structure and move to the interstitial position. At the interstitial position, Bi can undergo the following reaction and absorb an electron [31, 34];

$$\tfrac{1}{2}\,Bi_2O_3 \rightarrow \tfrac{3}{4}\,O_2 + Bi^* + P. \quad (3)$$

Bi^* is an ionized Bi atom in an interstitial site, and P is the charge of a positive hole. In this case, Bi behaves as an acceptor, dominates the donor effect, and decreases the conductivity. This reaction agrees very well with the conductivity behavior in the over-doped region (Bi>2.5 %). Anyway, the normal-state conductivity at room temperature σ_{300} is proportional to $n\tau$, where n is the carrier concentration and τ is the relaxation time, so Bi doping primarily has two different effects: the first is the increase of electron density and the other is the decrease of τ due to structural distortion induced by the doping [36]. In the under-doped region, structural distortion is very weak, and the change of τ can be neglected, so increasing n improves the conductivity. On the other hand, in the over-doped region, structural distortion may be strong and τ decreases markedly. As a result, the conductivity is decreased.

The potential energy of an electron in vacuum can be taken as zero. In practice, it represents a potential outside a surface at a distance smaller than the size of a sample, so we do not expect any problem due to the air gap between the surface of the samples and electrodes since we have inserted the samples in close contact with the electrodes. However, the disappearance/lack of these two nonlinear regions in the other samples support that no problem was created for/due to the contact between the samples and the electrodes [37].

The materials with features on the nanometer scale often have properties dramatically different from their bulk counterparts. The grain size of nanocrystalline materials is of the order of few nanometers so that about 40 to 80 % of the atoms are localized in the grain boundaries [38, 39]. They often have properties that are different compared to conventional microscale composites and can be synthesized using simple and inexpensive techniques. Therefore, the probability of Bi_2O_3 nanoparticle substitution into the grain boundaries of ZnO is very high at the considered sintering temperature. With increasing Bi content for nanoparticle samples, the nanosized grains are able to localize at the grain boundaries of ZnO and take part in producing some other sensitive intergrain conduction paths [40, 41]. These conduction paths can operate in parallel to the grain boundary region and slightly participate in deforming the potential barriers of nanosize grains in the low field region. With increasing field, the ZnO microsize grains are working as a varistors in the high-field region. This is in a good agreement with I–V characteristics where two nonlinear regions exist.

4 Conclusions

A comparative study of the effects of micro- and nano-Bi_2O_3 additions on $Zn_{1-x}Bi_xO$ varistors has been performed. We have shown that addition of Bi up to 5 % does not influence the hexagonal wurtizite structure of ZnO, while its grain size is affected. Furthermore, two nonlinear regions were obtained in the I–V curves of ZnO as a result of Bi_2O_3 nanoparticle additions above 5 %, but this behavior was completely absent in the samples containing microparticles. Moreover, the breakdown field and nonlinear coefficient could be increased up to 4,532 V/cm and 23.35, respectively, due to the addition of 20 % Bi_2O_3 nanoparticles. On the other hand, the electrical conductivity was increased by Bi additions up to 2.5 %, followed by a decrease with further increase of Bi content up to 20 %. It is suggested that the nanosized grains of Bi are localized at the grain boundaries of ZnO ceramics, producing additional sensitive conduction paths and completely deforming the potential barriers of ZnO varistors.

Acknowledgments The authors would like to thank the Deanship of Scientific Research, King Faisal University, Saudi Arabia for providing facilities and maintenance support during the Project no.: 140073.

References

1. J. Jose, K.M. Abdul, Mater. Sci. Eng. A **304–306**, 810 (2001)
2. D.C. Look, Mater. Sci. Eng. B **80**, 383 (2001)
3. L. Gao, Q. Li, W. Luan, H. Kawaoka, T. Sekino, K. Niihara, J. Am. Ceram. Soc. **85**(4), 1016 (2002)
4. D.R. Clarke, J. Am. Ceram. Soc. **82**(3), 485 (1999)
5. K. Mukae, K. Tsuda, I. Nagasawa, Jpn. J. Appl. Phys **16**(8), 1361 (1977)
6. G.E. Pike, C.H. Seager, J. Appl. Phys. **50**(5), 3414 (1979)
7. F. Obe, Y. Sato, T. Yamamoto, Y. Ikuhara, T. Sakuma, J. Am. Ceram. Soc. **86**(9), 1 (2003)
8. Z. Zhou, K. Kato, T. Komaki, M. Yoshino, H. Yukawa, M. Morinaga, K. Morita, J. Eur. Ceram. Soc. **24**, 139 (2004)
9. M. Matsouka, Jpn. J. Appl. Phys **10**(6), 736 (1971)
10. K. Eda, IEEE. Electr. Insul. Mag. **5**, 28 (1989)
11. J. Han, A.M.R. Senos, P.Q. Mantas, J. Eur. Ceram. Soc **22**, 1653 (2002)

12. D.C. Look, J.W. Hemsky, J.R. Sizelove, Phys. Rev. Lett. **82**, 2552 (1999)
13. W.G. Carlson, T.K. Gupta, J. Appl. Phys. **53**, 5746 (1982)
14. A. Sedky, M. Abu-Abdeen, A. Abdul-Aziz, Physica B **388**, 266 (2006)
15. A. Sedky, A. Ayman, A.M. Yassin, Physica B **404**, 3519 (2009)
16. Sedky A and El-Suheel E., Physics Research International **1** (2010)
17. E. Olsson, L.G. Dunlop, J. Appl. Phys **66**(9), 4317 (1989)
18. J. Wong, J. Appl. Phys. **51**(8), 4453 (1980)
19. T. Senda, C.R. Bradt, J. Am. Ceram. Soc **72**(8), 1541 (1990)
20. Y.M. Chiang, D.W. Kingery, M.L. Levinson, J. Appl. Phys. **53**(3), 1765 (1982)
21. R. Metz, H. Delalu, R.J. Vignalou, N. Achard, M. Elkhatib, Mater. Chem. Phys. **63**, 157 (2000)
22. M.A. Peiteado de la Rubia, M.J. Velasco, F.J. Valle, A.C. Caballero, J. Eur. Cream. Soc **25**, 1675 (2005)
23. T. Yamazaki, H. Yamada, K. Watanabe, K. Mitsuishi, Y. Toda, K. Furya, I. Hashimoto, Surf. Sci. **583**, 166 (2005)
24. M.L. Dinesha, H.S. Jayanna, S. Ashoka, G.T. Chandrappa, J. Alloy. Compd **485**, 538 (2009)
25. S.A. Shojaee, M.M. Shahraki, M.A.F. Sani, A. Nemati, A. Yousefi, J. Mater. Sci. Mater. Electron. **21**, 571 (2010)
26. A. Sedky, K.M. Mahfoz, Curr. Appl. Phys. **13**, 2117 (2013)
27. G. Pei, C. Xia, S. Cao, J. Zhang, W. Feng, J. Xu, J. Magn. Mag. Mater **302**(2), 340 (2006)
28. E. Kisi, M.M. Elcombe, Acta. Crystallogr. Sect. C. Cryst. Struct. Commun **C45**, 1867 (1989)
29. Ü. Özgür, A. Ya, I. Alivov, C. Liu, A. Teke, M.A. Reshchikov, S. Doğan, C.V. Avrutin, S.J. Cho, H. Morkoçd, J. Appl. Phys **98**, 041301 (2005)
30. V.V. Deshpande, M.M. Patil, V. Ravi, Ceram. Int **32**, 85 (2006)
31. M. Houabes, S. Bernik, C. Talhi, A. Bui, Ceram Int **29**(6), 783 (2005)
32. R. Parra, J.A. Varela, C.M. Aldao, M.S. Castro, Ceram Int **31**, 737 (2005)
33. T. Badapanda, V. Senthil, S.K. Rout, L.S. Cavalcante, A.Z. Simões, T.P. Sinha, S. Panigrahi, M.M. de Jesus, E. Longo, J.A. Varela, Curr. Appl. Phys. **11**, 1282 (2011)
34. T.K. Gupta, J. Mater. Res. **7**(12), 3280 (1992)
35. B. Tanmaya, C. Laécio Santos, G.E. da Luz Jr, B. Nouga Cardoso, A. Shahid, L. Elson, Metall. Mater. Trans. A **44**(9), 4296 (2013)
36. A. Sedky, A.A. Almulhem, S.S. Ibrahim, Smart Mater. Struct. **15**, N99 (2006)
37. Sedky A, Physica B **400**(2007), 1.
38. R.W. Siegel, Ann. Mater. Sci. **21**, 559 (1991)
39. H. Gleiter, Prog. Mater. Sci. **33**, 223 (1989)
40. J. Han, P.Q. Mantas, A.M.R. Senos, J. Eur. Ceram. Soc. **21**, 1883 (2001)
41. Azmi B. Z, Zahid R, Hashim M, Shaari A. H, Yunus A. H, Saion W. M. M., Am E J., Appl. Sci. **22** (2005) (Special Issue)